ChemPubSoc Europe

DOI: 10.1002/cssc.201500950

CHEMSUSCHEM Full Papers

Highly Soluble Benzo[ghi]perylenetriimide Derivatives: Stable and Air-Insensitive Electron Acceptors for Artificial Photosynthesis

Hung-Cheng Chen,[a] Chao-Ping Hsu,*[b] Joost N. H. Reek,*[a] René M. Williams,[a] and Albert M. Brouwer*[a]

A series of new benzo[ghi]perylenetriimide (BPTI) derivatives has been synthesized and characterized. These remarkably soluble BPTI derivatives show strong optical absorption in the range of $\lambda = 300$–500 nm and have a high triplet-state energy of 1.67 eV. A cyanophenyl substituent renders BPTI such a strong electron acceptor ($E_{red} = -0.11$ V vs. the normal hydrogen electrode) that electron-trapping reactions with O_2 and H_2O do not occur. The BPTI radical anion on a fluorine-doped tin oxide | TiO_2 electrode is persistent up to tens of seconds ($t_{1/2} = 39$ s) in air-saturated buffer solution. As a result of favorable packing, theoretical electron mobilities (10^{-2}–10^{-1} $cm^2V^{-1}s^{-1}$) are high and similar to the experimental values observed for perylene diimide and C_{60} derivatives. Our studies show the potential of the cyanophenyl-modified BPTI compounds as electron acceptors in devices for artificial photosynthesis in water splitting that are also very promising non-fullerene electron-transport materials for organic solar cells.

Introduction

Perylene-3,4,9,10-tetracarboxylic acid diimide derivatives (perylene diimides, PDIs) are well-known dyes and pigments with widespread application in industry.[1] As a result of their outstanding photochemical stability and possibilities for chemical functionalization,[2] they have been investigated intensively in academic research on luminescent solar concentrators,[3] biolabeling and -imaging,[4] building blocks for functional nanomaterials,[5] fluorophores for single-molecule spectroscopy,[6] etc. Self-assembled nanostructures of PDIs feature strong π–π stacking interactions between the perylene backbones and a good electron-accepting character because of the imide moieties.[7] Outstanding charge-transport properties were also found in functionalized PDIs.[8] For this reason they have been utilized intensively in various organic electronic applications, such as n-type semiconductors in organic field-effect transistors (OFETs),[9] and electron acceptors in organic photovoltaic cells (OPVs).[10,11]

PDIs have been considered as potential acceptors in bulk heterojunction organic solar cells to replace fullerene.[12] However, the solar energy conversion efficiencies obtained in conjugated polymers[13] or small-molecule[14] photovoltaic blends with PDIs were significantly lower than those with fullerene-based acceptors. Recently, ultrafast spectroscopy studies suggested that the low internal quantum efficiency is the result of fast geminate recombination at the low-band-gap conjugated polymer–PDI interface.[15] We also showed that geminate and nongeminate charge recombination mechanisms result in PDI triplet-state formation in pyrene/PDI thin-film blends.[16]

One reason for the lower efficiency is charge loss because the energy of the triplet excited state of a PDI [$E(T_1) \approx 1.2$ eV] is often below that of the charge-transfer state. Consequently, charge recombination from charged states to the triplet state of PDIs can be thermodynamically favorable and efficient. Theoretical work also indicates that fast charge recombination from the charge-transfer states to the lower-lying triplet state of a PDI can play a role in a phthalocyanine/PDI system.[17]

Recently, a high excited triplet-state energy [$E(T_1) \approx 1.68$ eV] was reported for benzo[ghi]perylenetriimide (BPTI), which has a more expanded π-conjugated backbone than PDI.[18] This value is even higher than that of fullerene systems such as C_{60} [$E(T_1) \approx 1.63$ eV][19] and [60]PCBM [$E(T_1) \approx 1.50$ eV].[20] Consequently, in the design of long-lived charge-transfer states,[21] the BPTI chromophore could potentially provide the solution to avoid triplet formation by charge recombination. Furthermore, as a result of the small dielectric constant ($\varepsilon_r \approx 2$–4) in organic solar cells, the large Coulombic attraction of photogener-

[a] H.-C. Chen, Prof. J. N. H. Reek, Dr. R. M. Williams, Prof. A. M. Brouwer
Van 't Hoff Institute for Molecular Sciences
University of Amsterdam
P.O. Box 94157
1090 GD Amsterdam (The Netherlands)
E-mail: A.M.Brouwer@uva.nl

[b] Prof. C.-P. Hsu
Institute of Chemistry
Academia Sinica
128 Section 2 Academia Road
Nankang, Taipei 11529 (Taiwan)

Supporting information and ORCID(s) from the author(s) for this article are available on the WWW under http://dx.doi.org/10.1002/cssc.201500950.

ated electron–hole pairs results in low quantum yields of separation into long-lived dissociated charges.[22] A recent theoretical study suggested that solar cells with over 20% power conversion efficiencies can be achieved by increasing the ε_r to 10 in the cell.[23,24] Although several factors, which include orientation, geometry, packing density, and molecular polarizability, can influence the dielectric response of molecule-based systems,[25] it was shown that the increase of the polarity of the building blocks is an effective approach to increase the dielectric constant of organic π-conjugated materials by amplifying the chemical polarity as well as the ground-state dipole moment. Molecular design strategies include the introduction of polar groups (e.g., fluorine atoms substituted on the chromophore backbone)[26] or side chains (e.g., ethylene glycol, nitrile, functionalized peptide)[27–29] into the molecular structure. Recently, Kulkarni et al. reported that a high dielectric constant (up to 16) of an organic π-conjugated material can be obtained from a parallel orientation of molecular dipoles ordered by a stacked supramolecular assembly of PDIs.[30] An impressively high dielectric constant of 15 was also obtained in a hyperbranched copper phthalocyanine polymer with a high molecular polarizability because of the presence of cyanophenyl groups.[31,32] Consequently, to design new BPTI derivatives, we took into account the large local dipole of the cyanophenyl moiety, which was introduced in the five-membered ring imide position on the BPTI backbone.

To improve the solubility and processability of PDI derivatives, substituents can be added at the N atoms or at the bay positions.[33–34] Unfortunately, the prevention of π–π stacking with these strategies affects the electronic material properties negatively. Firstly, the low crystalline order as well as the low delocalization of the electronic charge density in the acceptor phase causes donor/PDI blends to exhibit high barriers to charge-transfer state dissociation, certainly compared to fullerene-based acceptors.[35] Secondly, it also results in a large free volume in the donor–acceptor (D–A) interfacial region and thereby decreases the average D/A electronic coupling.[36]

Electron D/A molecular systems that can undergo efficient photoinduced electron transfer are among the key requirements for solar-to-fuel artificial photosynthesis.[37–39] Currently, synthetic D/A molecular system designs mostly include fullerenes, quinones, and aromatic imides as acceptors.[38–41]

To accomplish photosynthetic water oxidation in molecule-based artificial photosynthetic devices, a high electrochemical reduction potential of the electron donor (photosensitizer) radical cation, $E(D/D^{\bullet+})$ is required.[42–44] In other words, a rather poor electron donor should be employed. The reaction free energy criteria to achieve a high quantum yield of photoinduced charge separation in the assembled D/A molecular system then dictates the use of a strong electron acceptor.[45]

In the present work, we show that planar BPTI derivatives with a cyanophenyl substituent on the five-membered ring imide, and two alkyl groups on the six-membered imides, are excellent electron acceptors that combine a surprisingly good solubility with the possibility of favorable π stacking in the solid state that leads to good charge-transport properties (Scheme 1). The electrochemical and spectroscopic properties of these BPTI derivatives with different side chains were investigated. PDI-1, which is used extensively as an electron acceptor in solution-processed organic photovoltaics, was also studied for comparison.[46] Quantum-chemical calculations give an insight into the electronic structure, reorganization energy for electron transfer, and ground-state dipole moment of these BPTI derivatives and predict high electron mobilities. When bound to a fluorine-doped tin oxide (FTO)|TiO_2 electrode, BPTICNP-2 can act as an air- and water-stable negative-charge relay.

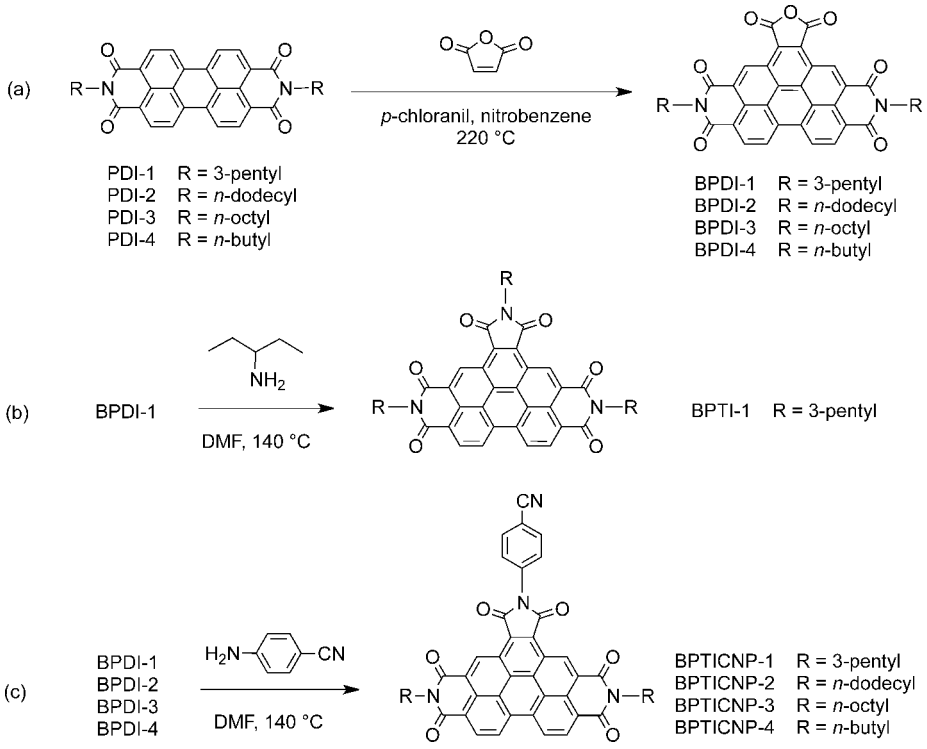

Scheme 1. Chemical structures and synthesis of BPTI derivatives through (a) Diels–Alder reactions on the PDI scaffold followed by substitution reactions with (b) 3-aminopentane or (c) 4-aminobenzonitrile.

Results and Discussion

Synthesis

To obtain our target BPTI compounds, we followed the conventional synthetic approach shown in Scheme 1[47,48] based on (a) Diels–Alder reactions on the PDI scaffold followed by substitution reactions with (b) 3-aminopentane or (c) 4-aminobenzonitrile. The reactions of the PDI derivatives PDI-1–PDI-4 and maleic anhydride in the presence of *p*-chloranil as an oxidizing agent result in the formation of diimido anhydrides BPDI-1–BPDI-4. Nitrobenzene was added to improve the solubility of the PDIs during the reaction with maleic anhydride.[49] As a result of the very poor solubility of BPDI-1–BPDI-4 in common solvents at room temperature, column chromatography purification could not be used. Dry crude BPDI-1–BPDI-4 were used directly after washing with methanol and acetone for the subsequent condensation reaction. During the condensation reactions, the complete dissolution of BPDI-1–BPDI-4 in hot DMF (~140 °C) was observed. In contrast to BPTICNP-4, the compounds BPTI-1, BPTICNP-1, BPTICNP-2, and BPTICNP-3 are all highly soluble at room temperature in common laboratory solvents such as dichloromethane, chloroform, THF, and DMF. The high room-temperature solubility of BPTICNP-2 and BPTICNP-3, which have no α-branched alkyl chains or bulky groups on the imide positions, is quite unusual. Particularly, the solubility of BPTICNP-2 in chloroform is up to 15 mg mL^{-1} (~15 mM) at room temperature, which is the required concentration for spin-coating in the fabrication of organic photovoltaic devices.[13] The length of the alkyl chains influences the solubility of BPTICNP-2–BPTICNP-4 in chloroform dramatically. A solubility of 15 mg mL^{-1} of BPTICNP-3 in chloroform can be achieved at ~50 °C in a hot-water bath (Figure S1). Unfortunately, BPTICNP-4 did not show suitable solubility in chloroform or other organic solvents such as *ortho*-dichlorobenzene, DMF, or THF at room temperature.

Steady-state spectroscopic studies

Room-temperature absorption and fluorescence spectra were measured to evaluate the electronic structure of the BPTI derivatives (Figure 1 and Table 1). Absorption spectra of PDI-1, BPTI-1, and BPTICNP-1–BPTICNP-3 in chloroform are shown in Figure 1 a. The benzo[ghi]perylene chromophore shows a blue-shifted absorption compared to that of the PDIs.[50] The typical vibronic fine structure of the strongly allowed benzo[ghi]perylene core π–π^* transitions ($\varepsilon_{466\,nm} \sim 6.2\times10^4$ cm^{-1} M^{-1}) on all BPTIs is apparent, and three bands at $\lambda = 467$, 436, and 410 nm were observed in the longer-wavelength region. The fact that all BPTI compounds have the same $S_0 \rightarrow S_1$ transition energy shows that the different alkyl groups on the imide and the presence of the cyanophenyl group do not influence the optical band gap. The absorption bands in the range of $\lambda \approx 350$–400 nm are assigned to the $S_0 \rightarrow S_2$ transition. There is a small redshift (635 cm^{-1}) on the $S_0 \rightarrow S_2$ transition of the BPTICNP analogues compared to BPTI-1. The transition dipole moment of $S_0 \rightarrow S_2$ is along the short-axis direction on BPTICNP, parallel to the direction of the cyanophenyl axis (blue arrow in Figure 1 c).

Table 1. Photophysical properties and triplet excited-state energies of PDI-1, BPTI derivatives, and fullerene derivatives C_{60}, [60]PCBM.

Compound	λ_{max}[a] [nm]	$\varepsilon\times10^{-4}$[a] [L mol^{-1} cm^{-1}]	λ_{em} [nm] S_1[b]	T_1[c]	$E(T_1)$ [eV] exp.[d]	theor.[e]
PDI-1	526	8.76	534	–	1.10[f]	1.24
BPTI-1	466	6.27	478	741	1.67	1.69
BPTICNP-1	466	6.24	479	741	1.67	1.68
BPTICNP-2	467	6.29	480	742	1.67	1.69
BPTICNP-3	467	6.29	480	–	–	1.69
C_{60}	–	–	–	–	1.63[g]	1.60
[60]PCBM	–	–	–	–	1.50[h]	1.53

[a] The longest wavelength absorption maxima. [b] Excitation wavelength $\lambda_{ex} = 480$ nm in PDI-1 and $\lambda_{ex} = 440$ nm in all BPTI derivatives. [c] Excited at 460 nm. [d] Derived from the maxima of the phosphorescence band. [e] Theoretical triplet-state energy from TDDFT calculations with B3LYP with the 6-31G(d) basis set. [f] Ref. [20] [g] Ref. [19]. [h] Ref. [20].

Figure 1 b. The normalized fluorescence spectra are shown in Figure 1 b. The substituents on BPTI have a negligible influence on the positions of the emission maxima.

The excited triplet-state energies of the BPTI analogues were determined from emission maxima in phosphorescence spectra in glassy matrices (2-methyltetrahydrofuran/iodoethane 1:1) at 77 K (Figure 2). The introduction of the polar cyanophenyl group in BPTICNP-1 or BPTICNP-2 does not result in any shift of the shortest-wavelength emission maxima. The phosphorescence band corresponds with a triplet excited-state energy of 1.67 eV for BPTI-1, BPTICNP-1, and BPTICNP-2. This value is very

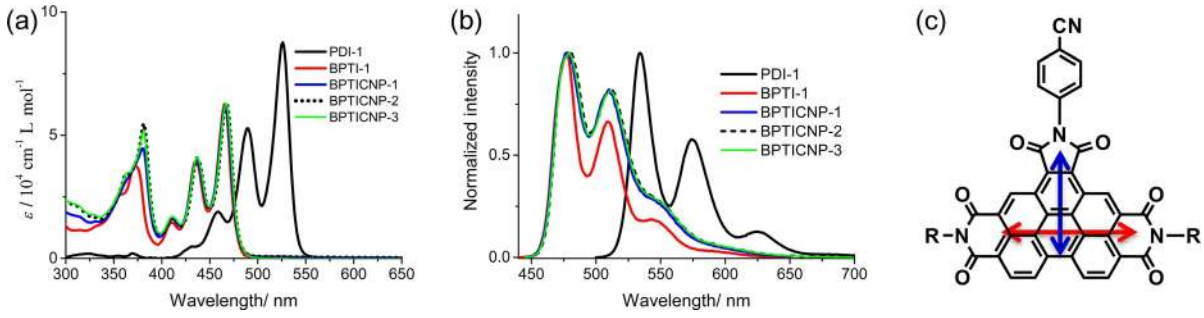

Figure 1. (a) UV/Vis absorption spectra and (b) fluorescence spectra of PDI-1 ($\lambda_{ex} = 480$ nm) and BPTI ($\lambda_{ex} = 440$ nm) derivatives in $CHCl_3$. (c) Transition dipole moments of BPTICNP. The red and blue arrows correspond to the $S_0 \rightarrow S_1$ and $S_0 \rightarrow S_2$ optical transitions, respectively.

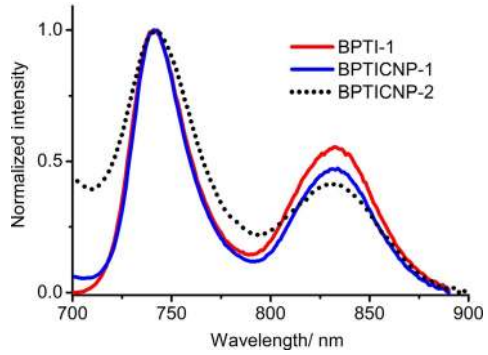

Figure 2. Corrected phosphorescence spectra ($\lambda_{ex}=460$ nm) of BPTI-1, BPTICNP-1, and BPTICNP-2 in 2-methyltetrahydrofuran/iodoethane (1:1) glass at 77 K.

similar to that of BPTI with branched alkyl side chains.[18] All spectral data are listed in Table 1. The T_1 energies of the BPTI compounds are 0.57 eV higher than that reported for *N*-hexylheptyl-substituted PDI.[20] Furthermore, the T_1 energies of BPTI compounds are higher by 40 meV than that of C_{60} [$E(T_1)\approx1.63$ eV][19] and 170 meV than that of [60]PCBM [$E(T_1)\approx1.50$ eV].[20] The theoretical triplet excited-state energies obtained with time-dependent density functional theory (TDDFT) calculations using the B3LYP functional with the 6-31G(d) basis set are also included in Table 1. The calculated T_1 energies of all BPTI compounds are in close agreement with the experimental values. These results indicate that TDDFT with B3LYP/6-31(d) is a good approach to calculate the triplet excited-state energy of BPTI compounds.

Spectro-electrochemical characterization of reduced BPTI

The radical anion species of BPTIs were produced by electrochemical reduction in dichloromethane at room temperature. The absorption spectra of the radical anions of BPTI-1, BPTICNP-1, and BPTICNP-2, are shown in Figure 3. In all cases, new broad bands appear during the reduction process with isosbestic points at $\lambda=480$ nm for BPTI-1, and BPTICNP-1 and $\lambda=486$ nm for BPTICNP-2. The spectral features of the radical anions are throughout the visible and near-infrared (NIR) regions, which all possess low-energy transitions that correspond to $D_0\rightarrow D_n$. The radical anion BPTI-1$^{\bullet-}$ shows four absorption bands with maxima at $\lambda=531$ ($\varepsilon=11200$), 644 (31100), 720 (15500), and 864 nm (13000 $M^{-1}cm^{-1}$) at an estimated conversion of ≈90%. In comparison with BPTI-1, the spectral features are not so clearly different for BPTICNP-1$^{\bullet-}$, which also displays four similar absorption bands with maxima at $\lambda=531$, 645, 721, and 864 nm. Clearly, the introduction of the cyanophenyl unit shifts the reduction potential to more positive values, but it does not induce spectral shifts in the radical anion spectra. The BPTICNP-2$^{\bullet-}$ radical anion also shows similar spectra with absorption bands with maxima at $\lambda=529$, 647, 717, and 856 nm and two enhanced shoulders at $\lambda=595$ and 762 nm.

Electrochemical studies

Cyclic voltammograms of PDI-1 and BPTI analogues in deaerated CH_2Cl_2 that contained 0.1 M NBu_4PF_6 are shown in Figure 4. For reasons of solubility, C_{60} was measured in toluene/1,2-dichloroethane (1:1) solution. The measured half-wave potentials $E_{1/2}$ are collected in Table 2. Ferrocene was used as an internal standard, and the ferrocene/ferrocenium redox couple has a half-wave potential $E_{1/2}=0.690$ V vs. the normal hydrogen electrode (NHE) in CH_2Cl_2. All potentials are related to the NHE.

Table 2. Redox properties and estimated LUMO energies of PDI-1, BPTI derivatives, and C_{60} from cyclic voltammetry.

Compound	$E_{1/2}$ [V vs. NHE]				E_{LUMO}[a] [eV]
	X/X^-	X^-/X^{2-}	X^{2-}/X^{3-}	X^{3-}/X^{4-}	
PDI-1	−0.39	−0.58	–	–	−3.77
BPTI-1	−0.41	−0.67	−1.29	–	−3.75
BPTICNP-1[b]	−0.21	−0.43	−0.64	−1.08	−3.95
BPTICNP-2[b]	−0.11	−0.42	−0.65	−1.09	−4.05
BPTICNP-3[b]	−0.10	−0.43	−0.64	−1.06	−4.06
C_{60}	−0.35	−0.73	−1.19	–	−3.81

[a] The potential of 0.24 V vs. NHE corresponds to 0.0 V vs. SCE. $E_{LUMO}=-(E_{[red\ vs.\ SCE]}+4.4)$ eV, Refs. [58, 59]. [b] The potential values are derived from DPV measurements.

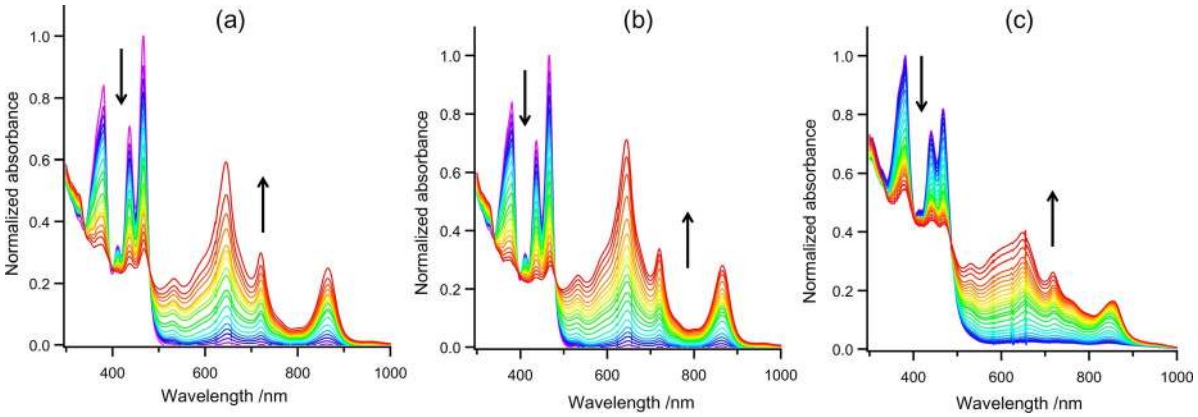

Figure 3. UV/Vis spectral changes in the first electron reduction of (a) BPTI-1, (b) BPTICNP-1, and (c) BPTICNP-2 in deaerated CH_2Cl_2 that contained 0.1 M NBu_4PF_6 (0.1 M).

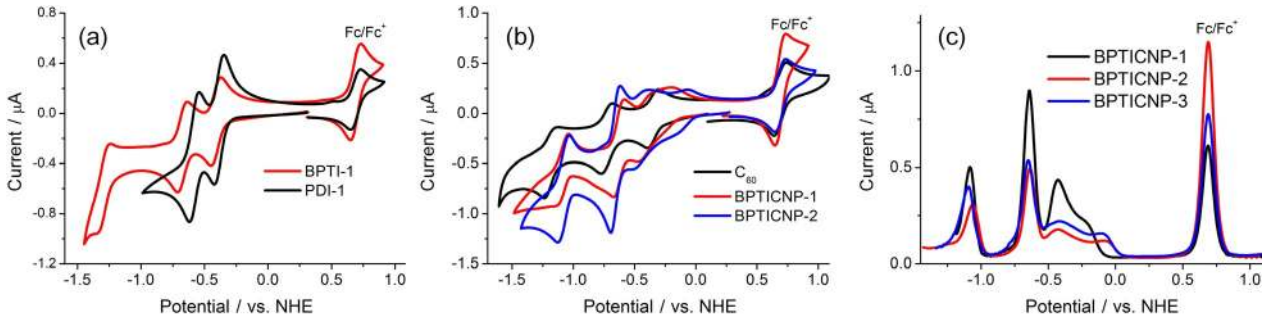

Figure 4. Cyclic voltammograms of (a) PDI-1 and BPTI-1 and (b) C_{60}, BPTICNP-1, and BPTICNP-2. (c) DPV of BPTICNP-1, BPTICNP-2, and BPTICNP-3 in deaerated CH_2Cl_2 solution with 0.1 M NBu_4PF_6 electrolyte. C_{60} was measured in toluene/1,2-dichloroethane (1:1). Sweep rate: 100 mV s^{-1} for CV and 5 mV s^{-1} for DPV. Fc/Fc^+ used as the internal standard, NHE = Fc/Fc^+ +0.69 V.

The first X/X^-, the second X^-/X^{2-}, and the third X^{2-}/X^{3-} redox couples of BPTI-1 were reversible and clearly detectable (Figure 4a). If we compare the first and second redox potentials of BPTI-1 and PDI-1, we can see that these values are only slightly negatively shifted in BPTI-1: the additional electron-withdrawing imide moiety on BPTI-1 does not improve the electron-accepting strength of BPTI. The results for C_{60} and cyanophenyl-substituted BPTI (BPTICNP-1 and BPTICNP-2) are shown in Figure 4b. Although the first redox waves are not identified clearly in BPTICNP-1 and BPTICNP-2, a gradual shift of the onset potential to more positive values can be observed on going from C_{60} to BPTICNP-2. This indicates that the cyanophenyl-substituted BPTIs have a stronger electron-accepting character than C_{60}. To obtain a clearer determination of the reduction potentials, differential pulse voltammetry (DPV) was applied to investigate BPTICNP-1, BPTICNP-2, and BPTICNP-3 (Figure 4c). The reduction potentials of these compounds are given in Table 2. Four clear reduction signals are observed in DPV.

To gain further insight into the electronic properties, the frontier molecular orbital (MO) energies of the PDI and BPTI compounds were calculated at the B3LYP/6-31G(d) level. The energy levels and the electron distributions of the HOMO and LUMO of the PDI and BPTI compounds calculated at the B3LYP/6-31G(d) level are depicted in Figure 5. The effect of the electron-withdrawing imides is mainly a reduction of the HOMO energy in BPTI-1. The LUMO energy of BPTI-1 is slightly higher than that of PDI-1, which is consistent with the slightly negative shift of the first redox potential. The electron-withdrawing cyanophenyl group participates in the electron capture on BPTIs, as shown by the delocalization of electron density to the cyanophenyl moiety in the LUMO (Figure 5). This shifts the first reduction potential by +200 mV if we compare BPTICNP-1 to BPTI-1. The replacement of the 3-pentyl group with *n*-alkyl chains induces a further positive shift (~100 mV). The first reduction potentials of BPTICNP-2 and BPTICNP-3 with linear alkyl chains are more positive (≈240–250 mV) than that of C_{60}. More importantly, BPTICNP-3 has its first reduction potential at −0.10 V vs. NHE, which is very close to that of the primary plastoquinone electron acceptor Q_A for which $E(Q_A/Q_A^{\bullet-}) = -0.08$ V vs. NHE in the photosynthetic reaction center.[51] The calculated energies (Figure 5) of the LUMO and HOMO shift by the same amount upon the introduction of the electron-withdrawing cyanophenyl group from BPTI-1 to BPTICNP-1. This leads to a constant HOMO–LUMO gap, in agreement with the optical absorption spectra.

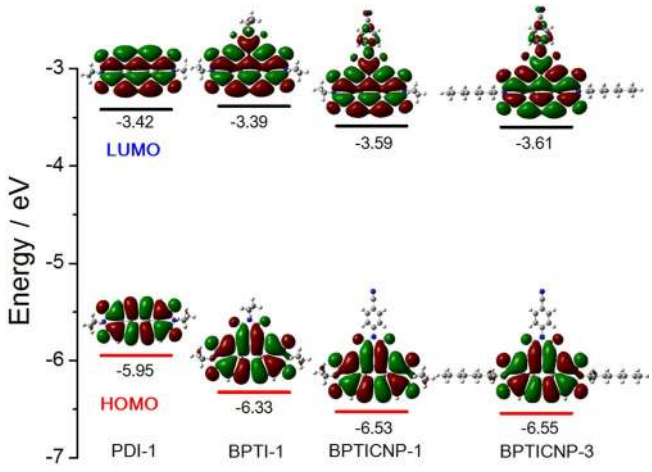

Figure 5. Theoretical calculated energy levels as well as frontier orbital (isovalue = 0.005) plots of PDI-1 and BPTI derivatives.

For long-term stability, all the active materials in organic heterojunction solar cells or in photoanodes based on a D/A molecular assembly for water splitting are required to be chemically stable in water- and oxygen-containing environments. The effects of water on the degradation of the photoactive material in organic solar cells have been reported.[52–54] A high degree of π-conjugation and alkyl side chains on photoactive materials can provide a hydrophobic interface that is water resistant. More importantly, the radical (di)anions of rylene diimide compounds are known to be remarkably chemically stable in a deoxygenated aqueous solution.[55–57]

Unfortunately, these radical (di)anions are converted immediately to the neutral parents upon exposure to air.[56] Likewise, serious electron mobility degradation was observed in PDI and fullerene derivatives for OFETs upon exposure to air.[59–61] This is a result of electron trapping by absorbed O_2 and water. To make n-type organic semiconductors resistant to O_2/H_2O electron traps, the tuning of the LUMO energy to −4.0 eV has been suggested as a design strategy.[59,60,62,63] In air-stable n-type OFETs based on rylene diimide derivatives, strong electron-withdrawing groups, such as –CN, –F, –Cl, and $–NO_2$,

have been incorporated on bay positions[59,64–66] or densely packed perfluoroalkyl chains were placed at the imide N,N′ positions to prevent H_2O and O_2 diffusion.[59] In fullerene derivatives, only [84]PCBM, which has a low-lying LUMO level of ~ −4.0 eV, shows air-stable electron-transport behavior.[67] The widely used [60]PCBM, C_{60}, and even [70]PCBM as electron acceptors in organic solar cells are not suitable for the design of photoanodes for direct water oxidation in aqueous solution. For our BPTI compounds, the experimental LUMO level energies derived from the reduction potentials are shown in Table 2 and are 0.4–0.5 eV more negative than the computed values, but show the same trend. BPTI-1 has $E_{LUMO} = -3.75$ eV, which is similar to the values of $E_{LUMO} = -3.77$ eV for PDI-1 and $E_{LUMO} = -3.81$ eV for C_{60}. Thus, it can be expected that the electron-transport performance of BPTI-1 will be sensitive to O_2 and H_2O. Functionalization of the BPTI core with the electron-withdrawing cyanophenyl group, however, results in lower LUMO energies: $E_{LUMO} = -3.95$ eV for BPTICNP-1 and $E_{LUMO} = -4.06$ eV for BPTICNP-2 and BPTICNP-3. Thus, the BPTICNP compounds are expected to be resistant to O_2/H_2O electron traps if they transport electrons through a BPTI film. Notably, although air-stable PDI-based OFETs have been obtained by functionalizing PDI cores with electron-withdrawing substituents and dense self-segregation of the perfluoroalkyl modification, the typically low triplet-state energy of PDI can still act as an energy sink in these PDI derivatives. Our BPTICNP compounds, however, show both a high triplet-state energy comparable to that of fullerene derivatives and $E_{LUMO} < -4.0$ eV. Thus, they satisfy the requirement for resistance to O_2/H_2O electron traps formulated for OFETs and also preclude triplet charge recombination processes. Both these advantages imply that BPTICNP can be a suitable electron acceptor phase for an organic photovoltaic-based photoanode for direct water oxidation.[68]

Furthermore, to investigate the stability of the radical anion of water-insoluble BPTI in air-saturated buffer solution, which is compatible with light-driven water oxidation conditions, a FTO|TiO_2|BPTICNP-2 electrode was prepared. The cyano group of the BPTICNP can act as an anchor by complexation to the Ti ions on the TiO_2 surface.[69] The surface coverage Γ of the BPTICNP-2 dye on the FTO|TiO_2|BPTICNP-2 electrode can be estimated from Beer's law, and a value of 1.31×10^{-8} mol cm^{-2} was obtained. This value is one order smaller than the typical value (~10^{-7} mol cm^{-2}) in conventional dye-sensitized solar cells.[70] Compared to the absorption spectra of BPTICNP-2 in chloroform, the loss of vibrational fine structure and a broader, redshifted spectrum of BPTICNP-2 on the electrode can be observed clearly (Figure 6a). This indicates that molecular aggregation of BPTICNP-2 occurs on the TiO_2 surface. In electrochemical studies of the FTO|TiO_2|BPTICNP-2 electrode in aqueous solution, the initial reduction wave of BPTICNP-2 is more positive (~200 mV) than that of trapped states of TiO_2 with a potential of −0.36 V vs. NHE (Figure S2). It can be concluded that electron transfer from the radical anion of BPTICNP-2 to TiO_2 will be thermodynamically unfavorable. Consequently, the BPTICNP-2 radical anion on the electrode can be prepared by the addition of the sacrificial reductant sodium dithionite ($Na_2S_2O_4$) in aqueous solution.

Upon immersion of the FTO|TiO_2|BPTICNP-2 electrode in a $Na_2S_2O_4$ solution, the electrode presented a yellow color initially and then gradually turned greenish. The spectral features of the greenish electrode are similar to those of the electrochemically generated BPTICNP-2 radical anion in CH_2Cl_2, which evidenced the formation of the radical anion of BPTICNP-2 on the electrode (Figure 6b and c). Notably, the saturated and steady absorbance of the radical anion was only observed in a large excess of $Na_2S_2O_4$. This phenomenon probably results from the spin-pairing effect in molecular aggregation, which prevents further reduction.[55,71] The aggregation stabilizes the radical anion species, which is also observed in PDI aggregation in solution and films.[72,73] Upon the immersion of the greenish FTO|TiO_2|BPTICNP-2 electrode in $Na_2S_2O_4$-free air-saturated phosphate buffer solution (pH 8.0, 0.1 M), the greenish electrode gradually turned yellow. The color change indicates that the BPTICNP-2 radical anion is oxidized slowly by the oxygen dissolved in water. The oxidation reaction was followed as a function of time by absorption spectroscopy, which shows a smooth conversion to the initial absorption spectrum of the neutral species (Figure S3). Importantly, the observed lifetime of the BPTICNP-2 radical anion is several tens of seconds (half-life $t_{1/2} = 39$ s). This long-lived BPTICNP-2 radical anion state present for seconds is the key requirement in the design of

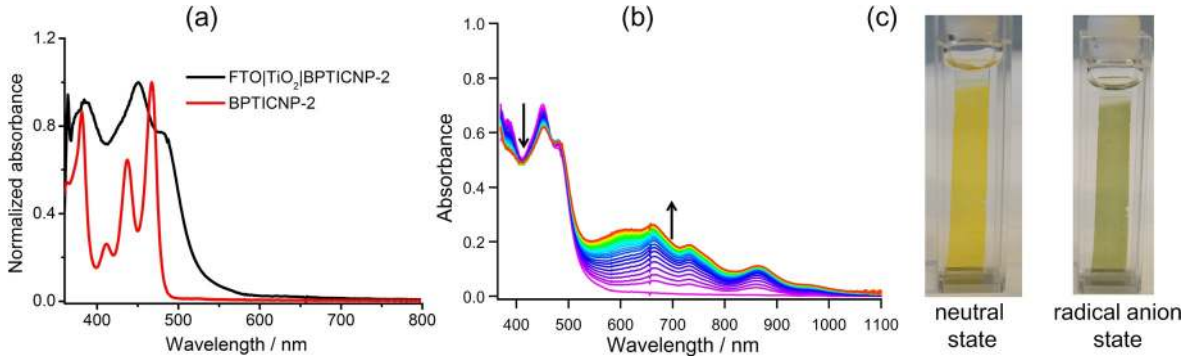

Figure 6. (a) Absorption spectra of the FTO|TiO_2|BPTICNP-2 electrode in water and BPTICNP-2 in chloroform. (b) Absorption spectra of the FTO|TiO_2|BPTICNP-2 electrode with 0.5 mM $Na_2S_2O_4$ in pH 8.0 KPi (0.1 M) buffer solution (5 s time difference between successive spectra. (c) Pictures of BPTICNP-2 in its neutral state and the radical anion state on the FTO|TiO_2|BPTICNP-2 electrode in aqueous pH 8.0 KPi (0.1 M) buffer solution.

long-lived charge transfer in a D/A assembly system in air-saturated buffer solution.

We found that the oxidation/reduction cycles can be repeated at least 10 times and we even repeated the reaction with a large excess of $Na_2S_2O_4$ for days in air without any noticeable BPTICNP-2 decomposition or desorption from the electrode. These results indicate that BPTICNP-2 can undergo full and reversible chemical charge/discharge of excess electrons and is chemically resistant to superoxide or its byproducts (e.g., H_2O_2) in air-saturated phosphate buffer solution.

Theoretical electronic structure and electron-transport properties

Increasing the dielectric constant can make free charge carriers separate more easily from the bound electron–hole pairs on the D–A interface. The molecular structure concept in the design of the desired dielectric properties should consider the net polarity of the molecular structure, as argued in the Introduction. To improve the molecular dielectric properties, the first step is to increase the dipole moment in the whole molecule.[30] The introduction of strongly polar groups or side chains into the molecular structure can be an effective approach. The computed ground-state dipole moments of PDI-1, BPTI, and fullerene derivatives (C_{60} and [60]PCBM) are listed in Table 3. The electrostatic potential (ESP) surface maps are presented in Figure 7 for further insights into the ground-state charge distributions. In PDI-3, even though ESP shows opposite colors between the imides and the perylene core, the resulting local dipoles still cancel each other out because of symmetry, which yields a zero dipole for PDI-1. In BPTI compounds, the five-membered ring imide enhances the ground-state dipole moment μ_g to 1.30 Debye in BPTI-1. Furthermore, a negative ESP is clearly present on the cyano moiety on the cyanophenyl group. This indicates that this extra dipole can extend from the bayside imide on BPTI backbone. Hence, the strongly polar cyanophenyl group dramatically enhances the μ_g to 7.76 Debye in BPTICNP-1 and 7.77 Debye in BPTICNP-3. These values are two times higher than that of [60]PCBM.

Table 3. Calculated internal reorganization energies for electron transfer (λ_{in}) and the ground-state dipole moment (μ_g) of PDI, BPTI, and fullerene derivatives.

Compound	λ_{in} [meV]	μ_g [D]
PDI-1	259	0
PDI-3	260	0
BPTI-1	247	1.3
BPTICNP-1	264	7.76
BPTICNP-3	263	7.77
C_{60}	140	0
[60]PCBM	149	3.44

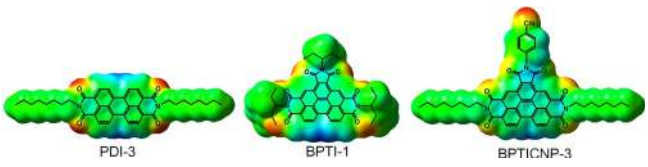

Figure 7. Electrostatic potential surfaces of PDI-1 and BPTI derivatives calculated at the B3LYP/6-31G (d) level of theory. The relatively negative (electron-rich region) electrostatic potential is highlighted in red, and the positive (electron-poor region) is highlighted in blue.

At the microscopic level of n-type organic semiconductors, the charge-transport mechanism can be described as involving an electron transfer from a charged organic acceptor molecule A^- to an adjacent neutral one A [Eq. (1)]:

$$A^- + A \rightarrow A + A^- \quad (1)$$

The basic assumption is that the charge is localized on a single molecule and charge migration takes place through an intersite hopping mechanism. In the context of semiclassical Marcus electron transfer theory,[74] the electron hopping rate k_{hop} can be estimated by Equation (2):[75]

$$k_{hop}(H_{RP}, \lambda, T) = \frac{2\pi}{\hbar} H_{RP}^2 \frac{1}{\sqrt{4\pi\lambda k_B T}} \exp\left[-\frac{\lambda}{4 k_B T}\right] \quad (2)$$

in which T is the temperature, H_{RP} is the electronic coupling matrix element that reflects the strength of electronic interaction in orbital overlap between the adjacent molecules in the electron self-exchange process, and λ is the overall reorganization energy, which includes external (λ_s) and internal (λ_{in}) reorganization energies. If we assume that these hops can be described as electron transfer from a charged (and relaxed) molecule to a nearby neutral molecule, we can estimate the electron mobility μ [$cm^2V^{-1}s^{-1}$] from the Einstein relationship [Eq. (3)]:

$$\mu = \frac{qd^2}{k_B T} k_{hop} \quad (3)$$

in which q is the elementary charge and d is the intermolecular distance between adjacent molecules.[76]

Thus, the theoretical electron mobility of organic semiconductors can be obtained from k_{hop} and an estimate of the intermolecular distance at a given temperature. The k_{hop} can be evaluated by quantum-chemical calculations of electronic coupling and reorganization energy. Herein, we set T to room temperature (298 K).

For the reorganization energy, λ_s corresponds to the polarization of the surrounding medium upon electron transfer in an organic solid-state system and this value is often assumed to be negligible.[77] Therefore, λ here is only the internal reorganization energy of the isolated active molecules that accounts for the changes in the geometry of the two acceptor molecules upon electron transfer. In the present model, the reorganization energy for electron transfer in Equation (2) can be expressed as follows [Eq. (4)]:[76–78]

$$\lambda_{in} = E^R(Q_P) - E^R(Q_R) = E^A(Q_{A^-}) + E^{A^-}(Q_A) - E^A(Q_A) - E^{A^-}(Q_{A^-}) \quad (4)$$

in which R is the reactant state and P is the final state, both of which are with an anionic and a neutral molecule A. Q_X indicates the optimal nuclear coordinates for state X, which can be A or A^-. $E^X(Q_X')$ indicates the energy of state X calculated at Q_X'.

The internal reorganization energies of PDI-1, BPTI, and fullerene derivatives (C_{60} and [60] PCBM) were also computed at the B3LYP/6-31G(d) level, and the results are collected in Table 3. To obtain optimal charge transport in organic semiconductor systems, the reduction in the reorganization energy is important. The calculated λ_{in} values of electron transfer in PDI-1 and PDI-3 are very close to those obtained in benchmark studies of PDI with alkyl side chains.[76] BPTI-1 possesses a slightly lower reorganization energy (~12 meV) than PDI-1. BPTICNP-1 and BPTICNP-3 have slightly higher reorganization energies (~17 meV) than BPTI-1. The increase of the reorganization energy in BPTICNP-1 or BPTICNP-3 is induced by the increase of the degree of the freedom upon the introduction of the cyanophenyl moiety. Particularly, the dihedral angle between the five-membered ring imide and the cyanophenyl moiety increases from 143° in the neutral state to 148° in the anion. As expected, all reorganization energies of the BPTI compounds are higher (≈98–124 meV) than the values for C_{60} and [60] PCBM.

Another key requirement to tune the charge hopping rate and subsequently, the charge mobility in organic semiconductors is to identify the correlations between effective electronic coupling and the molecular stacking structure. We further studied the relative configurations and electronic properties of possible π stacked dimers of BPTICNP-3, which we constructed from insights derived from the crystal structure of PDI-3. In the PDI-3 solid state, a slipped parallel structure with a 1.12 Å shift of the short axis, a 3.05 Å shift of the long axis, and an interplanar distance of 3.28 Å was observed.[79] In this geometry, there is a favorable electrostatic interaction between the negative surface potentials on four carbonyl groups and positive potentials on the bay area (Figure 7).[7] Moreover, there are strong π–π and van der Waals interactions from the aromatic perylene cores and linear alkyl chains on adjacent PDI molecules. We constructed the *anti* and *syn* conformations of slipped parallel stacking geometries of the BPTICNP-3 dimer and calculated the binding energy and electronic coupling with various displacement distances as shown in Figure S4 and Figure 8 (*anti*- or *syn*-BPTICNP-3 with respect to the arrangements of the cyanophenyl groups on two monomers). We fixed the π–π displacement between the two BPTICNP-3 planes at 3.5 Å, a common π–π stacking distance, and shifted the other two dimensions. The calculated binding energies, electronic couplings, and deduced electron mobilities of *syn*-BPTICNP-3 dimers at different relative positions are shown in Figure 8. For comparison, the energy and electronic coupling of a C_{60} dimer was also calculated. The slipped and translated structures of *syn*-BPTICNP-3 and C_{60} dimers are also shown in Figure 8. The binding energies of the ground-state stacking geometries are computed with DFT using the M06-2X functional with the 6-31G(d) basis set and further with a basis set superposition error (BSSE) correction.[80,81] Electronic couplings were calculated by the direct coupling method with the Hartree–Fock (HF) scheme and the 6-31G(d) basis set.[82–84]

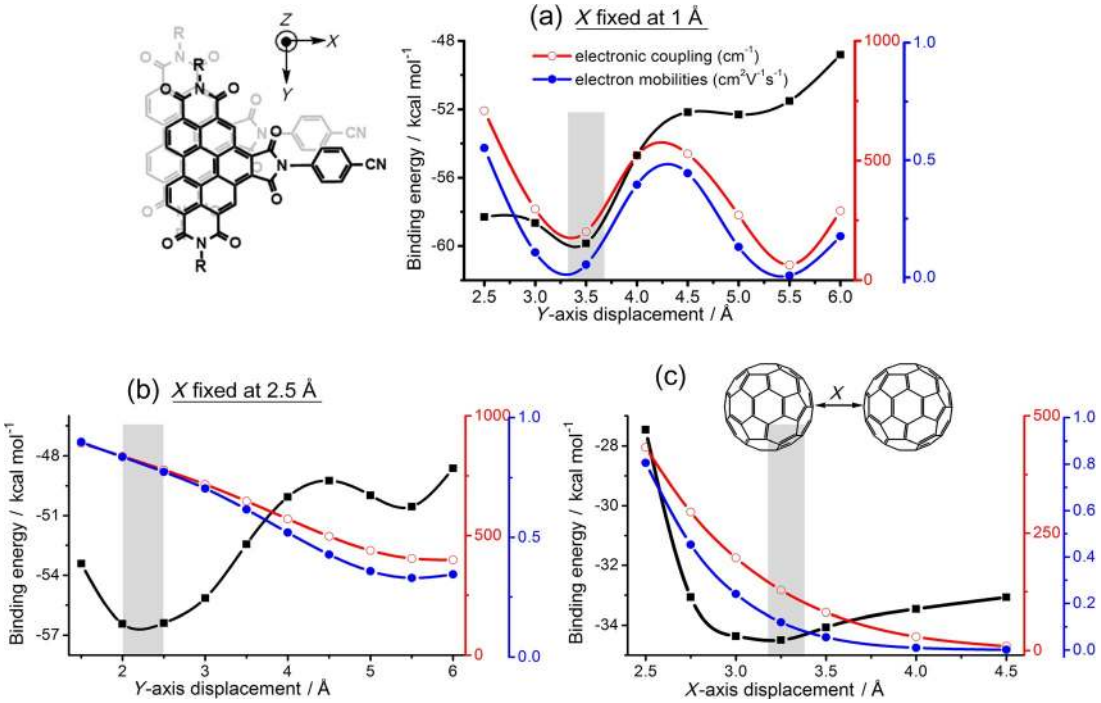

Figure 8. Calculated properties of the *syn* dimer of BPTICNP-3 and of the C_{60} dimer. Binding energies (kcal mol^{-1}; –■–), electronic couplings (cm^{-1}; –○–) and electron mobilities (cm^{2}V^{-1}s^{-1}; –●–) are shown as a function of *Y*-axis displacement for the BPTICNP-3 dimer (a, b) and as a function of intermolecular distance for C_{60} (c). To the left of (a) the structure of the dimer and the X, Y, and Z coordinates used are presented. The translated BPTICNP-3 is highlighted in black. For the *syn*-BPTICNP-3 dimer the interplanar distance (Z-axis) was fixed at 3.5 Å. A fixed shift along the X-axis was taken as 1 Å (a) or as 2.5 Å (b). The marked gray area represents the range of local minimum of binding energy.

The electrostatic interaction between the bayside imide and benzoperylene core and the strongly polar cyanophenyl group potentially promotes molecular interactions in the *syn* conformations of slipped parallel geometry. Therefore, we built two *syn* conformations with ΔX fixed at 1 and 2.5 Å (Figure 8a and b, respectively). By varying *Y*, binding energies $E_b = -59.8$ and -56.4 kcal mol^{-1} are obtained in the most stable dimer conformations (Figure 8a and b, respectively).

These E_b values are both more negative than those in *anti* conformations (see Figure S4). A fully optimized *syn*-BPTI dimer structure could be obtained from the geometry in Figure 8b. This optimal BPTI dimer structure is similar to that shown in Figure 8a and has $E_b = -69.9$ kcal mol^{-1}. This indicates that a barrierless pathway exists from the local minimal geometry shown in Figure 8b to that in Figure 8a.This favorable *syn* conformation of BPTICNP-3 indicates that unidirectional dipole moments can be obtained in the entire stacked BPTICNP-3 structure, which then lead potentially to a high dielectric constant.[85] The oscillation behavior of the electronic coupling shown in Figure 8a is caused by the alternating MO phase for the orbital overlap in charge transfer. High electron mobilities with values in the order of 0.05 ($H_{RP} = 202$) and 0.84 cm^{2}V^{-1}s^{-1} ($H_{RP} = 832$ cm^{-1}) can be obtained for the most stable conformations in Figure 8a and b, respectively. An electron mobility value of 0.06 cm^{2}V^{-1}s^{-1} ($H_{RP} = 243$ cm^{-1}) was obtained in the optimal *syn*-BPTICNP-3 dimer structure.

Notably, the calculated electron mobilities in the possible stacked BPTICNP-3 dimer conformations shown in Figure 8 are of the same order as the experimental ones in PDI derivatives with linear alkyl chains.[86–89] The C_{60} dimer with various displacement distances was also calculated, and the results are shown in Figure 8c. The local minima of the binding energy $E_b = -34.5$ kcal mol^{-1} can be observed at a translated distance with $\Delta X = 3.25$ Å, which is very close to the adjacent distance in the C_{60} crystal.[90] Our calculated electron mobility $\mu = 0.12$ cm^{2}V^{-1}s^{-1} ($H_{RP} = 128$ cm^{-1}) is in the range of the experimental values for C_{60}-based field-effect transistors.[91–94]

Conclusions

We have established the efficient gram-scale synthesis of benzo[ghi]perylenetriimides (BPTIs). Among these, BPTICNP-2 and BPTICNP-3, which have simple linear alkyl chains, are remarkably soluble in organic solvents (>15 mg mL^{-1}). The electrochemical and spectroscopic properties of these compounds were evaluated by cyclic voltammetry, differential pulse voltammetry, steady-state spectroscopy, and DFT calculations. The spectroscopic and electrochemical results were consistent with those of DFT calculations. High triplet-state energy levels of ~1.67 eV for BPTI compounds were found. These properties make them interesting components for bulk heterojunction solar cells or electron donor/acceptor molecular systems as compared to frequently used perylene diimides (PDIs), because triplet formation through charge recombination can be avoided. As expected, the introduction of the polar cyanophenyl group on the BPTI core unit not only improves the electron-accepting strength but also increases the ground-state dipole moment of the BPTI compounds. The addition of the cyanophenyl group on BPTI lowers the LUMO energy such that O_2/H_2O electron traps can be avoided in devices: the BPTICNP-2 radical anion on the fluorine-doped tin oxide (FTO)|TiO_2|BPTICNP-2 electrode showed a half-life $t_{1/2}$ of 39 s in air-saturated phosphate buffer solution. Importantly, the fully reversible chemical charge/discharge properties and chemical resistance to superoxide or its byproducts was found for the FTO|TiO_2|BPTICNP-2 electrode. From the theoretical investigation of the charge-transfer properties in BPTICNP-3 and C_{60}, we predict that BPTICNP-3 will reach similar electron mobilities to PDIs with linear alkyl chains and will also exhibit a comparable electron mobility to C_{60}. These findings will be explored in following studies as we believe that it will enable the design of new nonfullerene acceptors in solution-processed organic photovoltaics and assembled donor/acceptor molecular systems for artificial photosynthesis devices. Experimental confirmation of the dielectric constants and electron mobility in BPTICNP-2 and BPTICNP-3 will be established in future work.

Experimental Section

Photophysical measurements

UV/Vis absorption spectra were measured by using a HP/Agilent 8453 UV/Vis spectrophotometer using 10 mm path-length quartz cuvettes at RT. Emission spectra were measured by using a Spex Fluorolog 3 spectrometer equipped with double-grating monochromators in the excitation and emission channels. The excitation light source was a 450 W Xe lamp, and the detector was a Peltier cooled R636-10 (Hamamatsu) photomultiplier tube. The RT emission spectra were corrected for the wavelength response of the detection system. Phosphorescence measurements were performed at 77 K by using an Oxford Instruments liquid nitrogen DN 1740 cryostat equipped with an ITC4 control unit. Samples were degassed with three freeze–pump–thaw cycles at $\approx 10^{-5}$ mbar.

Electrochemical measurements

The electrochemical measurements were performed by using a potentiostat/galvanostat MacLab model ML160 controlled by NOVA software (1.8 version for Windows) using a conventional single-compartment three-electrode cell with a Pt working electrode, a Ag wire as the reference electrode, and a Pt wire as the counter electrode. All measurements in deaerated dichloromethane were performed with freshly distilled solvent with a solute concentration of $\approx$1.0 mM in the presence of NBu_4PF_6 (0.1 M) as the supporting electrolyte and a scan rate of 100 mV s^{-1} in cyclic voltammetry and 5 mV s^{-1} in DPV. Ferrocene (Fc) was added at the end of the experiment as internal standard to calibrate the redox potentials. The Fc/Fc$^+$ redox couple with a half-wave potential $E_{1/2}$ was set as 0.690 V vs. NHE in CH_2Cl_2.

Spectro-electrochemistry

UV/Vis spectro-electrochemistry was performed by using an optically transparent thin-layer (200 μm) electrochemical (OTTLE) cell equipped with CaF_2 optical windows and a Pt minigrid working electrode. The steady-state absorption spectra were recorded by using an HP1100 spectrometer in the course of the thin-layer cyclic voltammetry scanning process ($v = 2$ mV s^{-1}) controlled by a MacLab potentiostat with NOVA software. Solutions of BPTIs (1 mM) in dea-

erated dichloromethane that contained 0.1 M NBu_4PF_6 were used for the spectro-electrochemistry measurements.

Preparation of the FTO|TiO_2|BPTICNP-2 electrode

The FTO|nanostructured TiO_2 electrode was purchased from solaronix (ref. 73101). The FTO|TiO_2 electrode with a 3 cm×0.7 cm area was sensitized by soaking in a 1 mM solution of BPTICNP-2 dye in THF solution overnight at RT. Following sensitization, the electrode was rinsed with dichloromethane and dried at RT.

The estimated surface coverage Γ of BPTICNP-2 dye on FTO|TiO_2 [mol cm^{-2}] was calculated from UV/Vis measurements by Beer's Law using $\Gamma = A(\lambda)/(10^3 \times \varepsilon(\lambda))$, in which $A(\lambda)$ and ε (λ) are the absorbance and molar absorptivities at λ. If we used $\varepsilon = 6.29 \times 10^4$ cm^{-1} M^{-1} for BPTICNP-2 at 467 nm, the Γ of the FTO|TiO_2|BPTICNP-2 electrode was obtained as 1.31×10^{-8} mol cm^{-2}.

Spectro-electrochemistry of FTO|TiO_2|BPTICNP-2 electrode in aqueous solution

For the cyclic voltammetry measurements in aqueous solution, a three-electrode cell setup was used with the FTO|TiO_2|BPTICNP-2 electrode as the working electrode, a Pt wire counter electrode, and a Ag/AgCl 3 M KCl reference electrode. Values were converted to NHE potentials by using $E(\text{NHE}) = E(\text{Ag/AgCl}) + 0.197$ V. KH_2PO_4/K_2HPO_4 (0.2 M, pH 8.0) was the supporting electrolyte.

The stability of the radical anion of BPTICNP-2 in air-saturated phosphate buffer solution was investigated by time-resolved UV/Vis absorption spectroscopy. The absorption spectra of FTO|TiO_2 in 0.1 M, pH 8.0 potassium phosphate (KPi) buffer solution was set as the blank. The radical anion of BPTICNP-2 in aqueous solution was prepared by immersing the FTO|TiO_2| BPTICNP-2 electrode in 0.5 mM $Na_2S_2O_4$ in pH 8.0 KPi (0.1 M) buffer solution. After the reaction with $Na_2S_2O_4$ for 10 min in air, a steady concentration of the radical anion of BPTICNP-2 can be obtained by the observation of saturated absorbance in the UV/Vis absorption spectrum. The FTO|TiO_2|BPTICNP-2 electrode was transferred immediately to a UV/Vis cuvette with 4 mL of air-saturated pH 8.0 KPi (0.1 M) and $Na_2S_2O_4$-free buffer solution. The subsequent spectral evolution is shown in Figure S3.

Computational details

All computations were performed using a development version of Q-CHEM. All the molecules studied in the present work were fully optimized at the B3LYP/6-31G(d) level. The MOs and electrostatic potentials were calculated at the same level. Graphical outputs of the computational results were plotted using the Gauss View software program (ver. 3.09). For the excited-state calculation, we employed TDDFT with the B3LYP functional and 6-31G(d) basis set. The quantum-chemical binding energies were then calculated with a BSSE correction at the M06–2X functional with 6-31G(d) basis set [Eq. (5)].

$$E_{\text{binding}} = E_{\text{dimer}} - E_{\text{monomer+ghost}} \quad (5)$$

The dimer configurations were generated by moving the selected BPTICNP-3 or C_{60} to the desired relative positions. An optimal *syn*-BPTI dimer structure calculation was obtained by geometry optimization using the local minimal geometry shown in Figure 8b as the initial geometry and under DFT/M06-2X with the 6-31G(d) basis set calculation. The charge-transfer electronic coupling values of the dimer structure were evaluated by the direct coupling method, with wavefunctions obtained by the HF scheme and 6-31G(d) basis set.

Synthesis

The products were identified by ^{1}H and ^{13}C NMR spectroscopy (Bruker AMX 400) and field desorption mass spectrometry (FD-MS) performed by using an AccuTOF GC v 4g, JMS-T100GCV mass spectrometer equipped with an FD Emitter with an emitter voltage of 10 kV.

All PDI derivatives (PDI-1, PDI-2, PDI-3, and PDI-4) were obtained according to the literature: *N*^{1},*N*^{2}-bis(3-pentyl)-perylene-3,4,9,10-tetracarboxylic diimide (PDI-1),[95] *N*^{1},*N*^{2}-bis(1-dodecyl)perylene-3,4,9,10-tetracarboxylic diimide (PDI-2),[95] *N*^{1},*N*^{2}-bis(1-octyl)perylene-3,4,9,10-tetracarboxylic diimide (PDI-3),[96] and *N*^{1},*N*^{2}-bis(1-butyl)perylene-3,4,9,10-tetracarboxylic diimide (PDI-4).[97]

All BPDI derivatives (BPDI-1, BPDI-2, BPDI-3, and BPDI-4) were prepared using the same reaction conditions: *N*^{1},*N*^{2}-bis(3-pentyl) benzo[ghi]perylene-2,3,8,9,11,12-hexacarboxylic-2,3,8,9-bisimide-11,12-anhydride (BPDI-1), *N*^{1},*N*^{2}-bis(1-dodecyl)benzo[ghi]perylene-2,3,8,9,11,12-hexacarboxylic-2,3,8,9-bisimide-11,12-anhydride (BPDI-2), *N*^{1},*N*^{2}-bis(1-octy)benzo[ghi]perylene-2,3,8,9,11,12-hexacarboxylic-2,3,8,9-bisimide-11,12-anhydride (BPDI-3), and *N*^{1},*N*^{2}-bis(1-butyl)-benzo[ghi]perylene-2,3,8,9,11,12-hexacarboxylic-2,3,8,9-bisimide-11,12-anhydride (BPDI-4). A mixture of PDI (1.5 g), maleic anhydride (40 g), *p*-chloranil (5.0 g), and nitrobenzene (5 mL) was stirred at 220 °C for 24 h under a N_2 atmosphere. The progress of the reaction was monitored using the complete disappearance of the typical 525 nm absorption band of PDIs in chloroform or DMF. After cooling to RT, the deep-brown product solution was poured into methanol/ethyl acetate (1:1 v/v, 400 mL) and then sonicated for 30 min. The yellowish BPDI solid was collected by vacuum filtration and washed with methanol, ethyl acetate, and acetone. The dry crude BPDIs were used directly in the next reaction step.

N^1,N^2,N^3-Tris(3-pentyl))benzo[ghi]perylene-2,3,8,9,11,12-hexacarboxylic triimide (BPTI-1)

A mixture of the crude BPDI-1 (1.0 g, 1.6 mmol) and excess 3-aminopentane (1.5 mL, 13 mmol) in DMF (150 mL) was heated to 140 °C for 6 h under a N_2 atmosphere. The solution was cooled, and the reaction mixture was concentrated under reduced pressure. The yellow product was precipitated by the addition of methanol (100 mL). The precipitate was filtered and washed with methanol. The resulting residue was dissolved in chloroform and purified by column chromatography (silica gel, chloroform) to afford BPTI-1 (952 mg, 56% yield calculated from initial material PDI-1) as yellow powder. ^{1}H NMR (400 MHz, $CDCl_3$): $\delta = 10.44$ (s, 2H), 9.32 (d, 2H, $J = 8.0$ Hz), 9.12 (d, 2H, $J = 8.0$ Hz), 5.21–5.14 (m, 2H), 4.33–4.28 (m, 1H), 2.40–2.22 (m, 6H), 2.07–1.93 (m, 6H), 1.03–0.96 ppm (m, 18H); ^{13}C NMR (400 MHz, $CDCl_3$): $\delta = 168.91$, 133.42, 130.13, 128.02, 127.82, 127.35, 125.47 (br), 125.22, 125.05, 124.12, 123.62, 123.38 (br), 123.31 (br), 123.25 (br) 58.35, 56.59, 25.70, 25.26, 11.62, 11.58 ppm; FD-MS (10 kV): *m/z*: calcd for 693.2839: $C_{43}H_{39}N_3O_6$; found 693.2875.

N^1,N^2-Bis(3-pentyl)-N^3-(4-cyanophenyl)-benzo[ghi]perylene-2,3,8,9,11,12-hexacarboxylic triimide (BPTICNP-1)

A mixture of crude BPDI-1 (1.0 g, 1.6 mmol) and excess 4-aminobenzonitrile (760 mg, 6.4 mmol) in DMF (150 mL) was heated to 140 °C for 18 h under N_2. The solution was cooled, and the reaction mixture was concentrated under reduced pressure. The yellow product was precipitated by the addition of methanol (100 mL). The precipitate was filtered and washed with methanol. The resultant residue was dissolved in chloroform and purified by column

chromatography (silica gel, chloroform) to afford BPTICNP-1 (920 mg, 52% yield calculated from initial material PDI-1) as a yellow powder. ^{1}H NMR (400 MHz, $CDCl_3$): $\delta = 10.03$ (s, 2H), 9.03–8.96 (m, 4H), 8.03–7.93 (m, 4H), 5.18–5.12 (m, 2H), 2.40–2.30 (m, 4H), 2.15–2.04 (m, 4H), 1.07–1.03 ppm (m, 12H); ^{13}C NMR (400 MHz, $CDCl_3$): $\delta = 166.24$, 135.50, 133.45, 132.63, 127.47, 127.41, 127.14, 126.26, 124.31, 123.90, 122.60, 118.56, 112.14, 58.70, 25.3, 11.82 ppm; FD-MS (10 kV): *m/z*: calcd for 724.2322: $C_{45}H_{32}N_4O_6$; found 724.2321.

N^1,N^2-*Bis(1-dodecyl)*-N^3-*(4-cyanophenyl)-benzo[ghi]perylene-2,3,8,9,11,12-hexacarboxylic triimide (BPTICNP-2)*

A mixture of crude BPDI-2 (1.0 g, 1.2 mmol) and excess 4-aminobenzonitrile (580 mg, 4.9 mmol) in DMF (150 mL) was heated to 140 °C for 12 h under N_2. The solution was cooled, and the reaction mixture was concentrated under reduced pressure. The yellow product was precipitated by the addition of methanol (150 mL). The precipitate was filtered and washed with methanol. The resultant residue was dissolved in chloroform and purified by column chromatography (silica gel, chloroform) to afford BPTICNP-2 (921 mg, 54% yield calculated from initial material PDI-2) as an orange powder. ^{1}H NMR (400 MHz, $CDCl_3$): $\delta = 9.68$ (s, 2H), 8.68–8.61 (m, 4H), 8.01 (s, 4H), 4.25 (t, 4H, $J = 8.0$ Hz), 1.87–1.77 (m, 4H), 1.4–1.20 (m, 36H), 0.87–0.84 ppm (m, 6H); ^{13}C NMR (400 MHz, $CDCl_3$): $\delta = 163.79$, 162.55, 162.04, 135.28, 133.49, 131.93, 129.91, 128.31, 127.08, 126.46, 125.97, 124.84, 123.71, 123.53, 122.74, 121.77, 118.43, 112.43, 41.43, 32.18, 31.17, 29.98, 29.95, 29.90, 29.69, 29.63, 28.31, 27.46, 22.94, 14.37 ppm; FD-MS (10 kV): *m/z*: calcd for 920.4512: $C_{59}H_{60}N_4O_6$; found 920.4508.

N^1,N^2-*Bis(1-octyl)*-N^3-*(4-cyanophenyl)-benzo[ghi]perylene-2,3,8,9,11,12-hexacarboxylic triimide (BPTICNP-3)*

A mixture of crude BPDI-3 (1.0 g, 1.4 mmol) and excess 4-aminobenzonitrile (670 mg, 5.6 mmol) in DMF (150 mL) was heated to 140 °C for 18 h under an N_2 atmosphere. The solution was cooled, and the reaction mixture was concentrated under reduced pressure. The yellow product was precipitated by the addition of methanol (150 mL). The precipitate was filtered and washed with methanol. The resultant residue was dissolved in chloroform and purified by column chromatography on silica gel with chloroform/acetone (20:1) to afford BPTICNP-3 (961 mg, 58% yield calculated from initial material PDI-3) as an orange powder. ^{1}H NMR (400 MHz, $CDCl_3$): $\delta = 9.73$ (s, 2H), 8.72–8.62 (m, 4H), 8.01 (s, 4H), 4.26 (t, 4H, $J = 8.0$ Hz), 1.87–1.77 (m,4H), 1.50–1.30 (m, 20H), 0.92–0.88 ppm (m, 6H); ^{13}C NMR (400 MHz, $CDCl_3$): $\delta = 165.83$, 162.62, 162.11, 135.31, 133.49, 132.03, 129.95, 128.42, 127.08, 126.60, 126.55, 126.03, 124.90, 123.80, 123.57, 122.79, 121.88, 112.35, 41.44, 32.12, 29.53, 28.31, 27.45, 22.94, 14.38 ppm; FD-MS (10 kV): *m/z*: calcd for 808.3261: $C_{51}H_{44}N_4O_6$; found 808.3417.

N^1,N^2-*Bis(1-butyl)*-N^3-*(4-cyanophenyl)-benzo[ghi]perylene-2,3,8,9,11, 12-hexacarboxylic triimide (BPTICNP-4)*

A mixture of crude BPDI-4 (0.5 g, 0.8 mmol) and excess 4-aminobenzonitrile (396 mg, 3.4 mmol) in DMF (150 mL) was heated to 140 °C under N_2. After 3 h, a yellow precipitate was observed. The reaction was continued for 6 h. After cooling to RT, the precipitate was filtered and washed with methanol, acetone and chloroform. BPTICNP-3 was isolated as a yellow powder (460 mg, 55% yield calculated from initial material PDI-4). ^{1}H NMR and ^{13}C NMR could not be recorded because of its extremely poor solubility. FD-MS (10 kV): *m/z*: calcd for 696.2009: $C_{43}H_{28}N_4O_6$; found 696.2046.

Acknowledgements

This work is part of the research programme of the Foundation for Fundamental Research on Matter (FOM), which is part of the Netherlands Organisation for Scientific Research (NWO). This research is financed in part by the BioSolar Cells open innovation consortium, supported by the Dutch Ministry of Economic Affairs, Agriculture and Innovation. We thank Dr. Bo-Chao Lin, Dr. Zhi-Qiang You, and Dr. Chou-Hsun Yang for helpful discussions in computational studies.

Keywords: electrochemistry · electron transfer · photosynthesis · pi interactions · water splitting

[1] E. B. Faulkner, R. J. Schwartz, *High Performance Pigments*, Wiley-VCH, Weinheim, **2009**.
[2] C. Huang, S. Barlow, S. R. Marder, *J. Org. Chem.* **2011**, *76*, 2386–2407.
[3] W. E. Benjamin, D. R. Veit, M. J. Perkins, E. Bain, K. Scharnhorst, S. Mcdowall, D. L. Patrick, J. D. Gilbertson, *Chem. Mater.* **2014**, *26*, 1291–1293.
[4] T. Weil, T. Vosch, J. Hofkens, K. Peneva, K. Müllen, *Angew. Chem. Int. Ed.* **2010**, *49*, 9068–9093; *Angew. Chem.* **2010**, *122*, 9252–9278.
[5] F. Würthner, *Chem. Commun.* **2004**, 1564–1579.
[6] M. W. Holman, D. M. Adams, *ChemPhysChem* **2004**, *5*, 1831–1836.
[7] Z. Chen, A. Lohr, C. R. Saha-Möller, F. Würthner, *Chem. Soc. Rev.* **2009**, *38*, 564–584.
[8] Y. Che, A. Datar, X. Yang, T. Naddo, J. Zhao, L. Zang, *J. Am. Chem. Soc.* **2007**, *129*, 6354–6355.
[9] F. Würthner, M. Stolte, *Chem. Commun.* **2011**, *47*, 5109–5115.
[10] C. Li, H. Wonneberger, *Adv. Mater.* **2012**, *24*, 613–636.
[11] E. Kozma, M. Catellani, *Dyes Pigm.* **2013**, *98*, 160–179.
[12] A. F. Eftaiha, J.-P. Sun, I. G. Hill, G. C. Welch, *J. Mater. Chem. A* **2014**, *2*, 1201–1203.
[13] V. Kamm, G. Battagliarin, I. A. Howard, W. Pisula, A. Mavrinskiy, C. Li, K. Müllen, F. Laquai, *Adv. Energy Mater.* **2011**, *1*, 297–302.
[14] A. Sharenko, C. M. Proctor, T. S. van der Poll, Z. B. Henson, T.-Q. Nguyen, G. C. Bazan, *Adv. Mater.* **2013**, *25*, 4403–4406.
[15] D. W. Gehrig, I. A. Howard, V. Kamm, H. Mangold, D. Neher, F. Laquai, *J. Phys. Chem. C* **2014**, *118*, 20077–20085.
[16] R. M. Williams, N. Vân Anh, I. H. M. van Stokkum, *J. Phys. Chem. B* **2013**, *117*, 11239–11248.
[17] T. Kawatsu, V. Coropceanu, A. Ye, J.-L. Bredas, *J. Phys. Chem. C* **2008**, *112*, 3429–3433.
[18] B. Ventura, H. Langhals, B. Böck, L. Flamigni, *Chem. Commun.* **2012**, *48*, 4226–4228.
[19] J. W. Arbogast, A. P. Darmanyan, C. S. Foote, Y. Rubin, F. N. Diederich, M. M. Alvarez, S. J. Anz, R. L. Whetten, *J. Phys. Chem.* **1991**, *95*, 11–12.
[20] D. Veldman, S. C. J. Meskers, R. A. J. Janssen, *Adv. Funct. Mater.* **2009**, *19*, 1939–1948.
[21] J. W. Verhoeven, *J. Photochem. Photobiol. C* **2006**, *7*, 40–60.
[22] T. M. Clarke, J. R. Durrant, *Chem. Rev.* **2010**, *110*, 6736–6767.
[23] L. J. A. Koster, S. E. Shaheen, J. C. Hummelen, *Adv. Energy Mater.* **2012**, *2*, 1246–1253.
[24] N. Camaioni, R. Po, *J. Phys. Chem. Lett.* **2013**, *4*, 1821–1828.
[25] H. M. Heitzer, T. J. Marks, M. A. Ratner, *ACS Nano* **2014**, *8*, 12587–12600.
[26] Y. Lu, Z. Xiao, Y. Yuan, H. Wu, Z. An, Y. Hou, C. Gao, J. Huang, *J. Mater. Chem. C* **2013**, *1*, 630–637.
[27] F. Jahani, S. Torabi, R. C. Chiechi, L. J. A. Koster, J. C. Hummelen, *Chem. Commun.* **2014**, *50*, 10645–10647.
[28] N. Cho, C. W. Schlenker, K. M. Knesting, P. Koelsch, H.-L. Yip, D. S. Ginger, A. K.-Y. Jen, *Adv. Energy Mater.***2014**, *4*, 1301857.
[29] R. J. Kumar, J. M. Macdonald, T. B. Singh, L. J. Waddington, A. B. Holmes, *J. Am. Chem. Soc.* **2011**, *133*, 8564–8573.

[30] C. Kulkarni, K. K. Bejagam, S. P. Senanayak, K. S. Narayan, S. Balasubramanian, S. J. George, *J. Am. Chem. Soc.* **2015**, *137*, 3924 – 3932.
[31] M. Guo, X. Yan, Y. Kwon, T. Hayakawa, M. Kakimoto, T. Goodson, *J. Am. Chem. Soc.* **2006**, *128*, 14820 – 14821.
[32] B. Lin, X. Xu, *Polym. Bull.* **2007**, *59*, 243 – 250.
[33] H. Langhals, R. Ismael, O. Yu, *Tetrahedron* **2000**, *56*, 5435 – 5441.
[34] H. Quante, P. Schlichting, U. Rohl, Y. Geerts, K. Müllen, *Macromol. Chem. Phys.* **1996**, *197*, 4029 – 4044.
[35] R. D. Pensack, C. Guo, K. Vakhshouri, E. D. Gomez, J. B. Asbury, *J. Phys. Chem. C* **2012**, *116*, 4824 – 4831.
[36] P. Erwin, M. E. Thompson, *Appl. Phys. Lett.* **2011**, *98*, 223305.
[37] S. Bensaid, G. Centi, E. Garrone, S. Perathoner, G. Saracco, *ChemSusChem* **2012**, *5*, 500 – 521.
[38] M. R. Wasielewski, *J. Org. Chem.* **2006**, *71*, 5051 – 5066.
[39] D. Gust, T. A. Moore, A. L. Moore, *Acc. Chem. Res.* **2009**, *42*, 1890 – 1898.
[40] D. Gust, T. A. Moore, A. L. Moore, *Acc. Chem. Res.* **2001**, *34*, 40 – 48.
[41] G. Bottari, G. De Torre, D. M. Guldi, *Chem. Rev.* **2010**, *110*, 6768 – 6816.
[42] G. F. Moore, J. D. Blakemore, R. L. Milot, J. F. Hull, H. Song, L. Cai, C. A. Schmuttenmaer, R. H. Crabtree, G. W. Brudvig, *Energy Environ. Sci.* **2011**, *4*, 2389 – 2392.
[43] H.-C. Chen, D. G. H. Hetterscheid, R. M. Williams, J. I. van der Vlugt, J. N. H. Reek, A. M. Brouwer, *Energy Environ. Sci.* **2015**, *8*, 975 – 982.
[44] M. T. Vagnini, M. W. Mara, M. R. Harpham, J. Huang, M. L. Shelby, L. X. Chen, M. R. Wasielewski, *Chem. Sci.* **2013**, *4*, 3863 – 3873.
[45] G. J. Kavarnos, N. J. Turro, *Chem. Rev.* **1986**, *86*, 401 – 449.
[46] L. Schmidt-Mende, A. Fechtenkötter, K. Müllen, E. Moons, R. H. Friend, J. D. MacKenzie, *Science* **2001**, *293*, 1119 – 1122.
[47] J. Kelber, M.-F. Achard, B. Garreau-de Bonneval, H. Bock, *Chem. Eur. J.* **2011**, *17*, 8145 – 8155.
[48] L. Perrin, P. Hudhomme, *Eur. J. Org. Chem.* **2011**, 5427 – 5440.
[49] H. Langhals, S. Poxleitner, *Eur. J. Org. Chem.* **2008**, 797 – 800.
[50] N. Nijegorodov, R. Mabbs, W. S. Downey, *Spectrochim. Acta Part A* **2001**, *57*, 2673 – 2685.
[51] H. Dau, I. Zaharieva, *Acc. Chem. Res.* **2009**, *42*, 1861 – 1870.
[52] F. C. Krebs, *Stability and Degradation of Organic and Polymer Solar Cells*, Wiley, Chichester, UK, **2012**.
[53] M. Hermenau, M. Riede, K. Leo, S. A. Gevorgyan, F. C. Krebs, K. Norrman, *Sol. Energy Mater. Sol. Cells* **2011**, *95*, 1268 – 1277.
[54] Q. Bao, X. Liu, S. Braun, M. Fahlman, *Adv. Energy Mater.* **2014**, *4*, 1301272.
[55] J.-F. Penneau, B. J. Stallman, P. H. Kasai, L. L. Miller, *Chem. Mater.* **1991**, *3*, 791 – 796.
[56] E. Shirman, A. Ustinov, N. Ben-Shitrit, H. Weissman, M. A. Iron, R. Cohen, B. Rybtchinski, *J. Phys. Chem. B* **2008**, *112*, 8855 – 8858.
[57] M. A. Iron, R. Cohen, B. Rybtchinski, *J. Phys. Chem. A* **2011**, *115*, 2047 – 2056.
[58] C. M. Cardona, W. Li, A. E. Kaifer, D. Stockdale, G. C. Bazan, *Adv. Mater.* **2011**, *23*, 2367 – 2371.
[59] B. A. Jones, A. Facchetti, M. R. Wasielewski, T. J. Marks, *J. Am. Chem. Soc.* **2007**, *129*, 15259 – 15278.
[60] T. D. Anthopoulos, G. C. Anyfantis, G. C. Papavassiliou, D. M. De Leeuw, *Appl. Phys. Lett.* **2007**, *90*, 122105.
[61] M. Chikamatsu, A. Itakura, Y. Yoshida, *Chem. Mater.* **2008**, *20*, 24 – 26.
[62] X. Zhan, A. Facchetti, S. Barlow, T. J. Marks, M. A. Ratner, M. R. Wasielewski, S. R. Marder, *Adv. Mater.* **2011**, *23*, 268 – 284.
[63] H. Usta, A. Facchetti, T. J. Marks, *Acc. Chem. Res.* **2011**, *44*, 501 – 510.
[64] R. Schmidt, M. M. Ling, J. H. Oh, M. Winkler, M. Könemann, Z. Bao, F. Würthner, *Adv. Mater.* **2007**, *19*, 3692 – 3695.
[65] M. Gsänger, J. H. Oh, M. Könemann, H. W. Höffken, A. M. Krause, Z. Bao, F. Würthner, *Angew. Chem. Int. Ed.* **2010**, *49*, 740 – 743; *Angew. Chem.* **2010**, *122*, 752 – 755.
[66] K. Y. Chen, T. J. Chow, *Tetrahedron Lett.* **2010**, *51*, 5959 – 5963.
[67] T. D. Anthopoulos, F. B. Kooistra, H. J. Wondergem, D. Kronholm, J. C. Hummelen, D. M. De Leeuw, *Adv. Mater.* **2006**, *18*, 1679 – 1684.
[68] T. Abe, K. Nagai, T. Ogiwara, S. Ogasawara, M. Kaneko, A. Tajiri, T. Norimatsu, *J. Electroanal. Chem.* **2006**, *587*, 127 – 132.
[69] T. Michinobu, N. Satoh, J. Cai, Y. Li, L. Han, *J. Mater. Chem. C* **2014**, *2*, 3367 – 3372.
[70] L. H. Nguyen, H. K. Mulmudi, D. Sabba, S. A. Kulkarni, S. K. Batabyal, K. Nonomura, M. Grätzel, S. G. Mhaisalkar, *Phys. Chem. Chem. Phys.* **2012**, *14*, 16182 – 16186.
[71] C. J. Zhong, W. S. V. Kwan, L. L. Miller, *Chem. Mater.* **1992**, *4*, 1423 – 1428.
[72] L. Zhong, F. Xing, W. Shi, L. Yan, L. Xie, S. Zhu, *ACS Appl. Mater. Interfaces* **2013**, *5*, 3401 – 3407.
[73] R. O. Marcon, S. Brochsztain, *Langmuir* **2007**, *23*, 11972 – 11976.
[74] R. A. Marcus, *Angew. Chem. Int. Ed. Engl.* **1993**, *32*, 1111 – 1121; *Angew. Chem.* **1993**, *105*, 1161 – 1172.
[75] J. L. Brédas, J. P. Calbert, D. A. da Silva Filho, J. Cornil, *Proc. Natl. Acad. Sci. USA* **2002**, *99*, 5804 – 5809.
[76] M. C. R. Delgado, E. Kim, S. Filho, J. Bredas, *J. Am. Chem. Soc.* **2010**, *132*, 3375 – 3387.
[77] Y. Olivier, V. Lemaur, J. L. Brédas, J. Cornil, *J. Phys. Chem. A* **2006**, *110*, 6356 – 6364.
[78] V. Lemaur, M. Steel, D. Beljonne, J.-L. Brédas, J. Cornil, *J. Am. Chem. Soc.* **2005**, *127*, 6077 – 6086.
[79] J. Vura-Weis, M. A. Ratner, M. R. Wasielewski, *J. Am. Chem. Soc.* **2010**, *132*, 1738 – 1739.
[80] S. Simon, M. Duran, J. J. Dannenberg, *J. Chem. Phys.* **1996**, *105*, 11024 – 11031.
[81] D. Vijay, H. Sakurai, G. N. Sastry, *Int. J. Quantum Chem.* **2011**, *111*, 1893 – 1901.
[82] A. Farazdel, M. Dupuis, E. Clementi, A. Aviram, *J. Am. Chem. Soc.* **1990**, *112*, 4206 – 4214.
[83] B.-C. Lin, C.-P. Cheng, Z.-Q. You, C.-P. Hsu, *Phys. Chem. Chem. Phys.* **2011**, *13*, 20704 – 20713.
[84] Y. Shao, L. F. Molnar, Y. Jung, J. Kussmann, C. Ochsenfeld, S. T. Brown, A. T. B. Gilbert, L. V. Slipchenko, S. V. Levchenko, D. P. O'Neill, R. A. DiStasio Jr., R. C. Lochan, T. Wang, G. J. O. Beran, N. A. Besley, J. M. Herbert, C. Y. Lin, T. Van Voorhis, S. H. Chien, A. Sodt, R. P. Steele, V. A. Rassolov, P. E. Maslen, P. P. Korambath, R. D. Adamson, B. Austin, J. Baker, E. F. C. Byrd, H. Dachsel, R. J. Doerksen, A. Dreuw, B. D. Dunietz, A. D. Dutoi, T. R. Furlani, S. R. Gwaltney, A. Heyden, S. Hirata, C.-P. Hsu, G. Kedziora, R. Z. Khalliulin, P. Klunzinger, A. M. Lee, M. S. Lee, W. Liang, I. Lotan, N. Nair, B. Peters, E. I. Proynov, P. A. Pieniazek, Y. M. Rhee, J. Ritchie, E. Rosta, C. D. Sherrill, A. C. Simmonett, J. E. Subotnik, H. L. Woodcock III, W. Zhang, A. T. Bell, A. K. Chakraborty, D. M. Chipman, F. J. Keil, A. Warshel, W. J. Hehre, H. F. Schaefer III, J. Kong, A. I. Krylov, P. M. W. Gill, M. Head-Gordon, *Phys. Chem. Chem. Phys.* **2006**, *8*, 3172 – 3191.
[85] D. Miyajima, F. Araoka, H. Takezoe, J. Kim, K. Kato, M. Takata, T. Aida, *Science* **2012**, *336*, 209 – 213.
[86] R. J. Chesterfield, J. C. McKeen, C. R. Newman, P. C. Ewbank, D. A. Da Silva Filho, J. L. Brédas, L. L. Miller, K. R. Mann, C. D. Frisbie, *J. Phys. Chem. B* **2004**, *108*, 19281 – 19292.
[87] A. L. Briseno, S. C. B. Mannsfeld, C. Reese, J. M. Hancock, Y. Xiong, S. A. Jenekhe, Z. Bao, Y. Xia, *Nano Lett.* **2007**, *7*, 2847 – 2853.
[88] F.-C. Chen, C.-H. Liao, *Appl. Phys. Lett.* **2008**, *93*, 103310.
[89] Y. Wen, Y. Liu, C. A. Di, Y. Wang, X. Sun, Y. Guo, J. Zheng, W. Wu, S. Ye, G. Yu, *Adv. Mater.* **2009**, *21*, 1631 – 1635.
[90] W. I. F. David, R. M. Ibberson, J. C. Matthewman, K. Prassides, T. J. S. Dennis, J. P. Hare, H. W. Kroto, R. Taylor, D. R. M. Walton, *Nature* **1991**, *353*, 147 – 149.
[91] A. L. Briseno, S. C. B. Mannsfeld, M. M. Ling, S. Liu, R. J. Tseng, C. Reese, M. E. Roberts, Y. Yang, F. Wudl, Z. Bao, *Nature* **2006**, *444*, 913 – 917.
[92] H. Li, B. C. K. Tee, J. J. Cha, Y. Cui, J. W. Chung, S. Y. Lee, Z. Bao, *J. Am. Chem. Soc.* **2012**, *134*, 2760 – 2765.
[93] K. Itaka, M. Yamashiro, J. Yamaguchi, M. Haemori, S. Yaginuma, Y. Matsumoto, M. Kondo, H. Koinuma, *Adv. Mater.* **2006**, *18*, 1713 – 1716.
[94] C. F. Sung, D. Kekuda, L. F. Chu, Y. Z. Lee, F. C. Chen, M. C. Wu, C. W. Chu, *Adv. Mater.* **2009**, *21*, 4845 – 4849.
[95] S. Demmig, H. Langhals, *Chem. Ber.* **1988**, *121*, 225 – 230.
[96] M. Murugavelu, P. K. M. Imran, K. R. Sankaran, S. Nagarajan, *Mater. Sci. Semicond. Process.* **2013**, *16*, 461 – 466.
[97] G. Boobalan, P. K. M. Imran, S. Nagarajan, *Spectrochim. Acta Part A* **2013**, *113*, 340 – 345.

Received: July 13, 2015
Published online on September 23, 2015

